BULLETIN OF THE POLISH ACADEMY OF SCIENCES
TECHNICAL SCIENCES, Vol. 71(4), 2023, Article number: e146236
DOI: 10.24425/bpasts.2023.146236

MECHANICAL AND AERONAUTICAL
ENGINEERING, THERMODYNAMICS

# A bioinspired optimization strategy: to minimize the travel segment of the nozzle to accelerate the fused deposition modeling process

**SRIDHAR S, ADITYA K, VENKATRAMAN R, and VENKATESAN M***

School of Mechanical Engineering, SASTRA Deemed University, Tamil Nadu, Thanjavur-613401, India

**Abstract.** The fused deposition modeling process of digital printing uses a layer-by-layer approach to form a three-dimensional structure. Digital printing takes more time to fabricate a 3D model, and the speed varies depending on the type of 3D printer, material, geometric complexity, and process parameters. A shorter path for the extruder can speed up the printing process. However, the time taken for the extruder during printing (deposition) cannot be reduced, but the time taken for the extruder travel (idle move) can be reduced. In this study, the idle travel of the nozzle is optimized using a bioinspired technique called "ant colony optimization" (ACO) by reducing the travel transitions. The ACO algorithm determines the shortest path of the nozzle to reduce travel and generates the tool paths as G-codes. The proposed method G-code is implemented and compared with the G-code generated by the commercial slicer, Cura, in terms of build time. Experiments corroborate this finding: the G-code generated by the ACO algorithm accelerates the FDM process by reducing the travel movements of the nozzle, hence reducing the part build time (printing time) and increasing the strength of the printed object.

**Key words:** additive manufacturing; fused deposition modeling; extruder path; ant colony optimization; build time.

## 1. INTRODUCTION

Material extrusion, sheet lamination, binder jetting, direct energy deposition, vat polymerization, powder bed fusion, and material jetting are the seven main technologies in additive manufacturing (AM). Modeling is the first step in the additive manufacturing process chain, which also includes STL (standard tessellation language) file conversion, machine setup, build, part removal, and post-processing. This is the standard procedure for all types of 3D printing technologies. Once the 3D CAD modeling is done it is converted to a standard 3D printable format (.STL file). The generated STL file is then sent to the slicer software [1], where it slices the 3D model according to three major settings namely print settings, filament settings, and printer settings. The single sliced layer of the 3D model has different subtypes like infill, shell, skin, skirt, and travel these individual subtypes are called as segments see Fig. 1. Here, infill is defined as the object density, usually expressed as a percentage between 0 and 100. The shell includes the wall and top/bottom layers. The wall covers the vertical outer part of a print layer. The top and bottom layers form the horizontal segments. The top and bottom layers are also labelled as "skin". The part build time (print time) is determined by the time it takes to print each segment in a layer. Extruder tool paths are recorded as a series of G-codes generated by the slicer software is fed into the FDM machine. The raw material for an FDM printer is a filament that is fed into the extruder under pressure, where it is melted using a hot end. A nozzle extrudes the melted filament, depositing it on the build surface as per the path generated by the G-code. The print head moves around without actually depositing material at random intervals (idle move). This movement is called "travel" in the terminology of 3D printing. In Fig. 1, the travel path of the nozzle without depositing material to the subsequent printing segment is depicted by the blue dashed lines. The printing process with more travel movements will take more time. In this article, preliminary research on reducing travel movements to speed up printing (build) time is proposed. A bioinspired technique called the "ant colony optimization strategy", pioneered by Colorni and Dorigo [2] is applied to the problem of finding the shortest possible path for a nozzle. The aim is to find the best route for the extruder to move through all the needed print segments without repeating any of them.

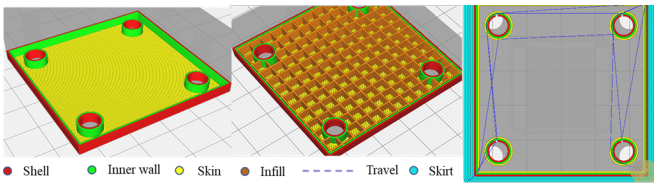


**Fig. 1.** Printing segments in a layer of a 3D object

The time required to print the object (build time) during the build stage is one of the major limitations of additive manufacturing technologies. The problem of determining the shortest travel path for the FDM process is presented. Heuristic al-

*e-mail: mvenkat@mech.sastra.edu

Manuscript submitted 2022-12-31, revised 2023-05-27, initially accepted for publication 2023-06-01, published in August 2023.

gorithms have been used to solve a variety of path generation problems, according to the literature. The algorithms proposed for solving the path optimization problem include genetic algorithm [3], travelling salesman problem [4], and neural networks [5]. Different methods were reported for path optimization in additive manufacturing. [6] used two hybrid algorithms namely, Greedy Two Optimizer and Greedy Annealing for reducing the total length of printing paths and overall printing time. The work was limited to simulations. [7] computationally tested a path planning algorithm using simple greedy option (the nearest neighbor method), and the combination of nearest and the farthest insertion method, to reduce the repositioning distance. The results show that using the two models it is possible to reduce the repositioning distance and it is observed that the distance is affected by the part geometry. [8] developed a path planning algorithm for an XY motion stage with an emphasis on aerosol printing to study printing time and material wasted. Trajectory planning is done using linear segments with parabolic blends, and printer transition was done using a minimum time trajectory planning. The study was limited to simulation and does not discuss the experimental validation of the proposed algorithm. [9] proposed a path-planning technique to reduce the number of sharp corners using an implicit algorithm derived from the level sets of input contours. The proposed method leads to a good surface finish compared to the standard fill patterns, which was validated using several examples and printed using a 3D printer. [10] proposed a fill path using fermat spiral for obtaining continuous filling to increase the speed of printing, and quality of the part. [11] presented a GA-based approach and a new strategy using a combination of the asymmetric TSP and integer programming (TSP-IP) to solve the problem. The performance of the heuristics is evaluated using simulated data, and it is found that they can significantly reduce the time wasted on non-machining motion. However, the paper does not provide a comparison of the proposed heuristics with other existing methods for solving the path-planning problem. [12] proposes a method for generating an infill geometry and path plan strategy for parts constructed with additive manufacturing, using Hilbert curves to minimize idle times and reduce both time and energy consumption. [13] proposed a stress-driven infill path planning for continuous fiber composite using wave function and TSP. Although several heuristics techniques were used for generating paths based on optimizing infill patterns, deposition sequence, and sharp edge reduction to obtain better surface finish, and time these studies also conclude that this affects the mechanical and surface properties.

[14] Ant colony optimization (ACO) is a metaheuristic optimization technique inspired by the behavior of ants searching for food. ACO algorithms were widely used in solving combinatorial optimization problems, the travelling salesman problem (TSP), the minimum spanning tree problem (MST), and the knapsack problem are examples of combinatorial optimization problems. ACO algorithms find the near-optimal solution faster so it was utilized in industrial applications where resource for computation and time is limited. [15] ACO has been applied successfully to a several number of path-finding problems in AM: [16] generated an optimized toolpath that reduces non-productive toolpaths in AM using ACO. Experimental results demonstrate the effectiveness of the proposed path-planning approach for both metal and non-metal parts. [17] proposed the use of ACO algorithm to solve undirected rural postman problems in 3D printing applications. It also suggests mechanisms to adaptively adjust the number of iterations of ACO to accelerate the printing process without affecting the quality of the solutions. The impact of the proposed mechanism on overall printing time is not detailed. Optimizing the transitions of the nozzle were also studied in FDM. A relaxation scheme for TSP-based 3D printing optimizer was proposed by [18] to reduce computational complexity. The results show that proposed scheme can reduce processing time significantly. [19] proposed a method to minimize number of transitions in nozzle-based 3D printing using direction-parallel line segments. An oriented mutation method (GA) is designed for the TSP to generate paths with fewer transitions which improves print quality. The presented work is based on GA, which may not always guarantee the optimal solution. Recently, ACO-based tool-path optimizer is proposed by [20] for 3D printing applications. The proposed method can improve visual quality by ignoring the stringing problem and reducing print time and presents experimental results that verify the effectiveness of the optimizer. It is observed that the study may not be suitable for all types of AM processes and mechanical properties were not included. A discrete event simulation is used by [21] to model the printing process for numerous possible travel paths to find optimal travel path which minimizes the formation of weak bonds. The work considers the time elapsed between successive printing of concrete layers and does not take into account other factors that affect structural integrity. An intelligent path-planning algorithm is proposed in [22] using TSP to reduce number and length of printing paths. The study compares the results with traditional path-planning algorithms and found that the proposed method significantly reduces number of paths, idle travel distance, and number of head lifts. Several other optimization algorithms have been used to optimize path-planning problems in 3D printing but focused especially on filling patterns and transitions. There is a need to optimize the travel segment alone in FDM printing process to reduce time as well as focus on the mechanical properties of the printed part.

The high build time in FDM printing is because of the travel segment of the nozzle which is a non-printable move. It is measured as the distance which the nozzle must travel between adjacent printed segments without extruding material. The travel segment can be substantial, especially in complex geometries, resulting in longer printing times. Therefore, there is a need for an optimization strategy which can minimize the travel segment of the nozzle and accelerate the overall printing speed with reduction in build time. The objective of the present work is to utilize a novel bioinspired optimization strategy that minimizes the travel segment of the nozzle during FDM printing. The approach combines principles from ant colony optimization with path-planning algorithms to dynamically adjust the printing path based on the object being printed.

In this study the optimal path obtained (G-code) from the ACO algorithm is compared with the path obtained (G-code)

by commercial slicer software Cura using the same printing parameters. Five case studies are printed to perform the experiment, and comparing the build time of the ACO-generated G-code with the G-code created from the commercial software. To determine the strength of the printed parts an ASTM standard tensile test is performed and the results have been analyzed.

## 2. PROBLEM DEFINITION

The domain of the problem is restricted to FDM systems, where the movement of the nozzle while printing a layer is obtained by X-Y movement. Further, the assumption is made that the data of a layer is presented using a sliced format (STL). Since all the layered manufacturing techniques use the same format which contains the information of the slice. In the FDM process, the nozzle passes through the segments in a layer and deposits filament (print move). After depositing filament in a segment, the nozzle should move from one reference to another reference without extruding the filament (travel). During travel (idle motion), the nozzle moves rapidly from the current reference point to another reference.The print segments (infill, wall, skin, travel, skirt) present in a layer of the sliced 3D object using the commercial slicer software [1] and the respective estimated build time is shown in Fig. 2. Each segment within a layer consumes time at a variable rate as shown in Fig. 2, for the 3D model the travel segment consumes 5% [1] of the printing time and by reducing travel movement the printing time can be reduced.

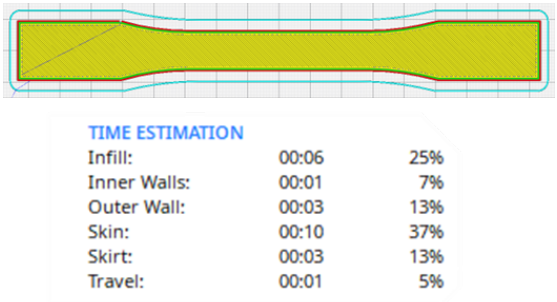


**Fig. 2.** Printing segments contribute to printing time for the 3D model based on cura

The problem is therefore stated as follows: (a) The printing segments in a layer are initially classified into domains based on the print move and travel move. (b) the nozzle should visit each coordinate only once during printing a segment in a layer. (c) the most recent printing segment coordinate is used as the start of the next reference point. As a result, the travel of the nozzle again to the reference point for the consecutive segment is avoided. In addition, the segments like infill, shell (inner and outer walls), skin, and skirt are not included in the optimization study, as each of these segments should deposit filament. Instead, the print order of each segment is optimized i.e. printing order of infill and shell segments are optimized as domains and the domains are connected using domain routes to have minimum travel.

## 3. PROBLEM FORMULATION

An ACO-based solver is proposed to minimize the build time. The proposed algorithm is a nature-inspired metaheuristic and can handle TSP [15] during the search. The procedure begins with the generation of G-code by a slicer software [1]. An algorithm is developed using the ACO technique with TSP which is written in MATLAB [23]. The procedure of the commercial slicer software to fabricate a 3D model is shown in Fig. 3a. The workflow begins with designing using CAD software [24, 25] or importing a 3D model from an online library [26]. The CAD model is converted to an stl file and transferred to slicer software like Ultimaker Cura, Makerbot, Formlabs, and Stratasys. Printing parameters such as layer thickness, infill percentage, raster angle, printing temperature, retraction, and fan speed are then configured. Slicing involves cutting the 3D object into sections (layer) of the specified thickness. Each section of the sliced 3D model includes data such as the model layer count and the types of printing segments, such as infill, shell, skin, and travel. The information of each layer is saved in the form of G-code, a machine language which can be recognized by the printer. Finally the generated G-code is fed to the FDM machine to perform 3D printing.

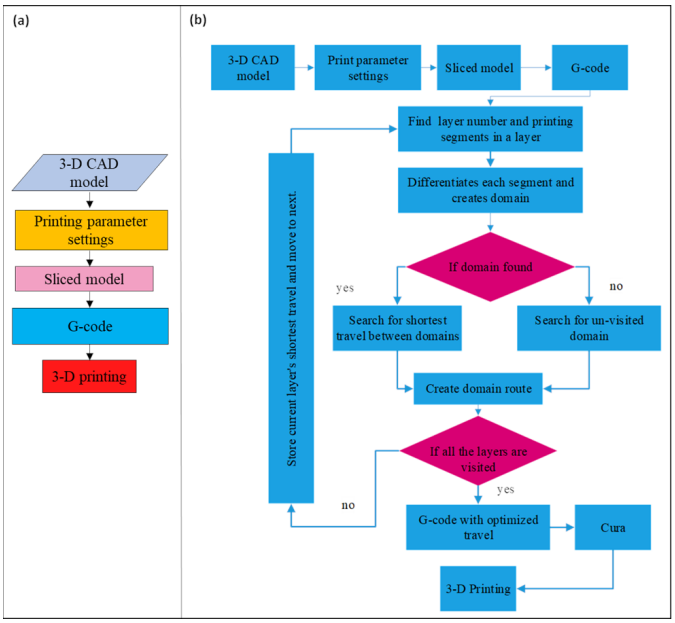


**Fig. 3.** Workflow of (a) Cura slicer and (b) proposed ACO solver

### 3.1. Domain creation

The layered architecture of the proposed method is shown in Fig. 3b. The workflow of the proposed method follows the procedure as the commercial slicer up to the generation of G-code. Since the G-code controls the printer actions it includes movement of the nozzle, extruder temperature, layer change, starts and pauses. The information in the generated G-code shown in Fig. 4 is converted to a text file and transferred to MATLAB [23]. Initially the solver search for the number of layers and print segments and saves the coordinates of each segment in a layer of a 3D model in the form of a matrix. The input

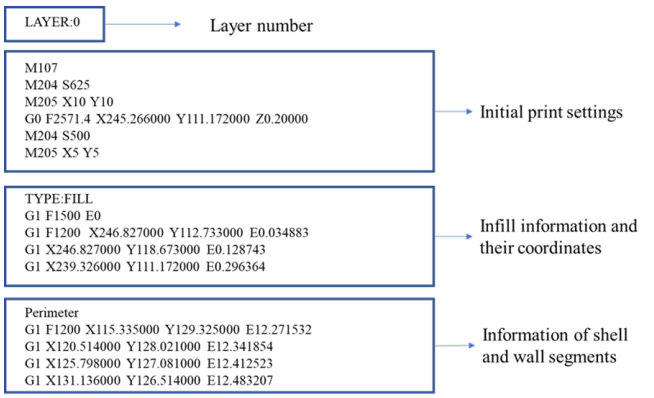


**Fig. 4.** G-code information about different segments in a sliced layer of a dogbone model

matrix has four columns as shown in Fig. 5, the x and y coordinates of the 3D model are in the first and second columns. The third column defines the type of segment: 1 for the infill and 2 for the shell. In the fourth column, based on the extrusion parameter in the G-code value 1 represents the printable segment and 0 represents travel. The coordinates of each segment type are stored in a separate matrix called the domain. The domain is defined in this context as a series of continuous printable and non-printable (travel) segments. To find the shortest path, the problem is transformed into a traveling salesman problem (TSP) [4, 15].

inputMatrix =

| X- coordinate | Y- coordinate | Segment type | Print and travel |
|---|---|---|---|
| 67.7380 | 214.8160 | 1.0000 | 1.0000 |
| 64.9100 | 214.8160 | 1.0000 | 1.0000 |
| 60.5600 | 210.4660 | 1.0000 | 1.0000 |
| 60.5600 | 213.2950 | 1.0000 | 1.0000 |
| 62.0810 | 214.8160 | 1.0000 | 0 |
| 79.8000 | 215.1780 | 2.0000 | 1.0000 |
| 60.2000 | 215.1780 | 2.0000 | 1.0000 |
| 60.2000 | 85.5780 | 2.0000 | 1.0000 |
| 79.8000 | 85.5780 | 2.0000 | 1.0000 |
| 79.8000 | 215.1780 | 2.0000 | 0 |
| 101.6790 | 214.8160 | 1.0000 | 1.0000 |
| 100.5590 | 213.6960 | 1.0000 | 1.0000 |
| 100.5590 | 210.8680 | 1.0000 | 1.0000 |

**Fig. 5.** Input matrix

### 3.2. Ant colony optimization for TSP

Ant Colony Optimization (ACO) is based on the ants' foraging behavior, notably their ability to find the quickest paths between food sources and their colony. It was first introduced [14] to solve Traveling Salesman Problem (TSP), each artificial ant looks for a set of boundaries that can be taken in order to find the tour length. The ants then deposit pheromones along the paths they have discovered. The amount of pheromone deposited is related to the length of the tour: the shorter the tour, the more pheromone is deposited since less pheromone has evaporated. The pheromone level is indicated as $\tau_{i,j}$ in which $i$, $j$ are vertices of the edge $(i, j)$, and $\eta(i, j)$ indicates the heuristic value which is inversely proportional to the interval among the vertices of an edge $(i, j)$. For every iteration, based on the path generated by every artificial ant, the pheromone matrix gets updated. The probability of the $k$-th ant located at a vertex $i$ to choose the next step $j$ can be calculated by equation (1).

$$p_{i,j}^{k}(t) = \frac{[\tau_{ij}(t)]^{\alpha}[\eta_{ij}]^{\beta}}{\sum_{l \in N_i^k}[\tau_{i,l}(t)]^{\alpha}[\eta_{i,l}]^{\beta}}. \tag{1}$$

Here, $N\_i^k$ represents the vertices set for the $k$-th ant to take the next valid unvisited vertice, $\alpha$ and $\beta$ are the parameter control for ACO. At every cycle end, an operation known as evaporation occurs which lowers the pheromone concentration along all edges. The pheromone level on the edge $(i, j)$ at the $t$-th iteration can be calculated as shown in equation (2)

$$\tau_{i,j}(t+1) = (1-\rho)\tau_{i,j}(t) + \sum_{k=1}^{m}\Delta\tau_{ij}^{k}(t). \tag{2}$$

Here, the number of artificial ants is $m$ and $\rho$ is the pheromone evaporation rate. For the edges having low pheromone levels, iteratively in the long run. After the path construction by the ants, the pheromones are updated. This is done by reducing the values of pheromones using a constant, and the pheromones are added to the routes where the ants crossed. The pheromone evaporation rate is implemented using equation (3)

$$\tau_{ij} = (1-\rho)\tau_{ij},\ \forall(i, j). \tag{3}$$

The pheromone evaporation rate is $\rho = 0.1$. To avoid more concentration of pheromones on the edges evaporation rate is limited to $0 < \rho \leq 1$. After evaporation, the ants start to deposit pheromones on the edges they passed during the tour using equation (4).

$$\tau_{ij} = \sum_{k=1}^{m}\Delta\tau_{ij}^{k},\ \forall(i, j). \tag{4}$$

The algorithm gives much importance to the print moves rather than travel by increasing pheromone levels. The value of the pheromone further decreases and is not included in the formation of the fastest route. The pheromone concentration on printable edges remains high. Figure 6 shows the formulation of the

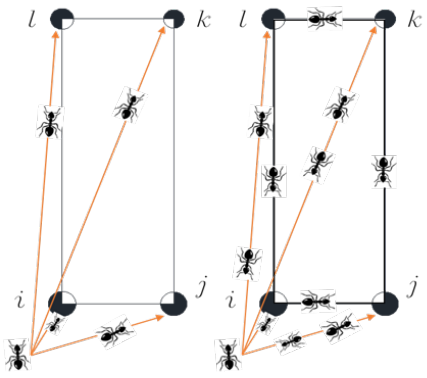


**Fig. 6.** Schematic of domains and domain routes created using ACO in a layer

problem based on ACO and TSP for nodes $(i, j, k, l)$ in a domain to find the shortest tour. The artificial ants search for the shortest travel between the nodes in the domain and based on the pheromone trails the domain routes for the shortest path are updated. This process continues up to the last layer of the model and the domain routes are stored and connected based on the printing segments and converted as G-codes for processing.

Five 3D models shown in Fig. 7a–e, Fin, Four-legged stool, Lego cube, Maze and, ASTM D- 638 dogbone specimen, are taken as the case study models for the present work. The models were chosen based on certain geometric features like (i) has large surface area, (ii) intricate shapes, and (iii) projections, where the nozzle have more travel segments. With the aid of Figs. 8a–h, the technique of the cura slicer and proposed solver

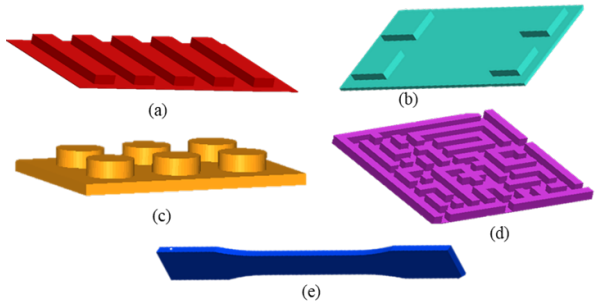


**Fig. 7.** 3D objects (a) Fin; (b) Stool; (c) Lego cube; (d) Maze; (e) Dogbone specimen

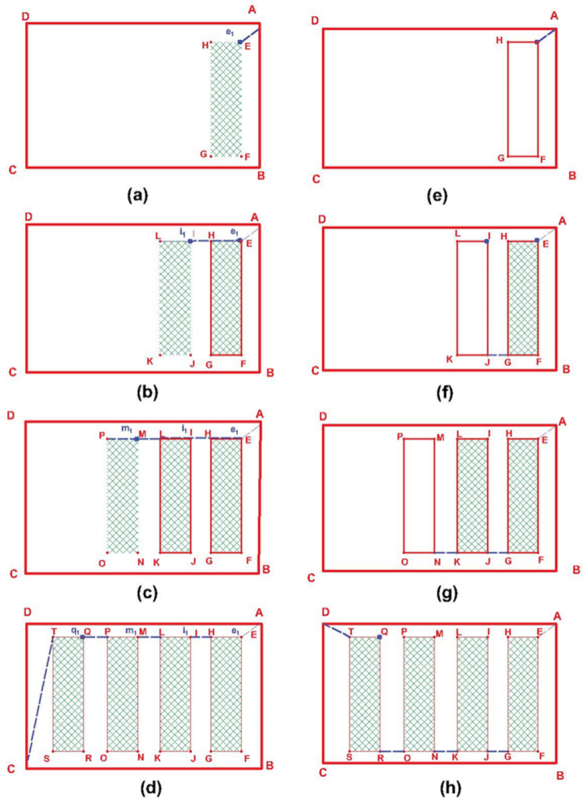


**Fig. 8.** Schematic representation of nozzle path generated for fin model (a)–(d) Cura Software, (e)–(h) ACO solver

was elucidated using the fin model. Here, the nozzle path is denoted by a series of printing motions (red) and travel movements (blue). Figure 8a illustrates that at A, the nozzle begins depositing material along the outer boundary B-C-D-A (thick red lines), producing the shell. The nozzle is then shifted to E from A. Here, in the g-code of the commercial slicer, the infill is initially filled within the wall EFGH, and then the material is deposited in the sequence E-F-G-H-E. Figure 8b shows the nozzle moving to the next sequence I-J-K-L-I from e1 (the blue dashed line) after finishing the segment EFGHE.

Figures 8c and d illustrate the sequence M-N-O-P-M and Q-R-S-T-Q for the print segments and i1, m1, and q1 for the travel segments of the current layer. Upon completion of the sequence Q-R-S-T-Q, it has been noticed that the nozzle returns to C via q1. The cycle continues until the final layer of the model is 3-D printed. The nozzle path developed by the proposed solver is illustrated in the above Figs. 8e–h. Figure 8e shows the nozzle depositing material in the sequence B-C-D-A to build the shell. The nozzle is then moved from A to E, as indicated in Fig. 8e (the blue dashed lines). In contrast to Fig. 8a, the proposed solver deposits material for the shell and wall segments as E-F-G-H-E, and then the infill is filled within the wall EFGHE, as shown in Fig. 8f.

The infill terminates at point G, and the proposed solver searches for the nearest printable segment from G, which is discovered to be J, as illustrated in Fig. 8f and deposits material in the sequence J-I-L-K-J. Figures 8g and h show the layer next segments print sequence N-M-O-P-N and R-Q-T-S-R. As shown in Fig. 8h upon finishing the print segments in the current layer the nozzle travels to the nearest point D to begin deposition on the next layer. The process continues until the algorithm reaches the last layer.

## 4. ACO IMPLEMENTATION AND EXPERIMENTS

The MATLAB code is executed on a computer with a 3.30 GHz Intel Core Xenon Processor, RAM of 128 GB, and the operating system as Windows 10. ACO-related parameters are selected from [27]. Table 1 lists the parameters used in the proposed method and for printing. The printing of the mentioned components using the proposed method and Cura software is done and compared. Experiments are carried out to determine the performance of the proposed method. The number of print segments and travel segments of the models are listed in Table 2.

It is to note here that all models do not have the same number of layers. The 3D models are sliced using an open-source slicing software called Ultimaker Cura [1] with default print settings. 20% infill density is chosen from the slicer for filling, with a constant speed of 60 mm/s [28]. The strength of the printed components (using two different G-codes) is tested. The solver performance is evaluated by testing the standard specimen [29] ASTM D638. A total of six specimens were printed using Acrylonitrile Butadiene Styrene (ABS) thermoplastic material. Three specimens were printed with the G-codes generated using Cura software and three specimens printed with the G-codes of the proposed solver. To reduce the random error the mean value of the tensile strength has been considered.

**Table 1**
Parameters used in Proposed ACO method, and printing settings

| Number of iterations | Number of ants | $\alpha$ | $\beta$ | $\rho$ | Infill density % | Layer height mm | Travel speed mm/s | Print speed mm/s | Printing temperature °C |
|---|---|---|---|---|---|---|---|---|---|
| 100 | 100 | 1 | 3 | 0.2 | 20 | 0.2 | 120 | 60 | 240 |

**Table 2**
Number of layers and travel segment for the considered models

| Model | Number of layers | Print segments | Travel segments |
|---|---|---|---|
| Four-legged stool | 49 | 9016 | 1813 |
| Fin | 54 | 28998 | 2484 |
| Lego cube | 124 | 81840 | 7192 |
| Maze design | 54 | 90072 | 13986 |
| ASTM tensile specimen | 16 | 2924 | 221 |

The samples are subjected to a uni-axial tensile test using Tinius Olsen H50KL Tensile testing machine with a load cell capacity of 500 kN and a displacement rate of 2 mm/min.

## 5. RESULTS AND DISCUSSION

The travel path of the nozzle determined by Cura software relatively consumes more time when compared to the ACO method. This can be visualized in Fig. 9a showing the path of the nozzle derived from the slicer Cura for the 3D fin model, the lines in black represent the nozzle travel movement. Figure 9b shows the path of the nozzle after ACO implementation, it is evident that the ACO method minimizes the travel transitions. The 3D stool model is shown in Figs. 9c and d before and after ACO implementation. Figures 9e and f, show the path of the lego cube, and Figs. 9g and h represent the maze design path. Figures 9i and j show the nozzle path obtained for an ASTM specimen before and after the implementation of ACO. The estimated time, total print time, and the number of travel (non-printable moves) for each of the case studies after printing using Cura and the ACO method are listed in Tables 3 and 4.

### 5.1. Estimated printing time

Table 3 contrasts the expected printing times of G-codes developed in Cura versus the ACO algorithm. The predicted printing time is evaluated using G-code analyzer [30], free and open-source software. G-code analyzer is utilized just for predicting printing time. It has been seen that the G-code generated by utilizing the proposed method results in a shorter estimated printing time compared to the G-code developed via the Cura software. Here the estimated time, and actual printing time are measured in seconds (s). Table 3 shows that the suggested methods work effectively for the Four-legged stool model, resulting in a 20% reduction in printing time compared to cura. The predicted time of fin model is 13% faster, as compared to cura, followed by the Lego model at 9%, the maze at 8%, and the ASTM tensile specimen at 11%. The outcomes demonstrate that the proposed method yields a shorter predicted time compared to the commercial slicer software cura.

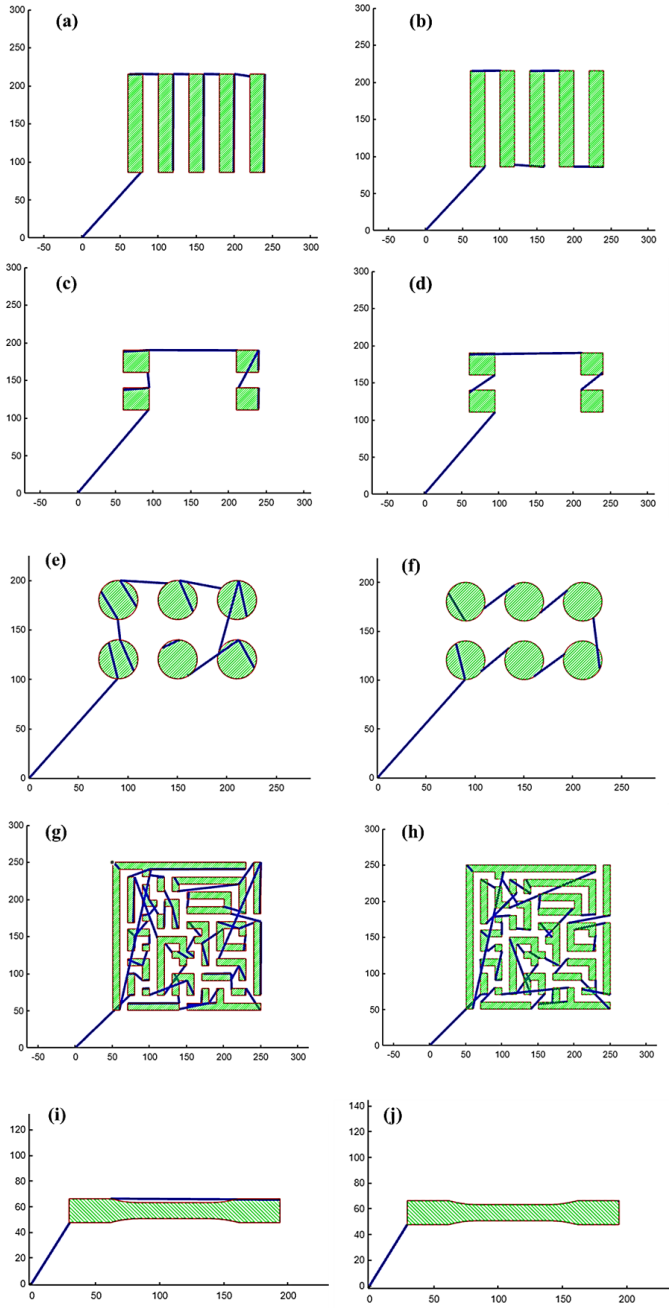


**Fig. 9.** Comparison of the Nozzle path generated from: (a), (c), (e), (g), and (i) Cura; (b), (d), (f), (h), and (j) proposed ACO algorithm

**Table 3**
Estimated printing time

| Model | Slicer (s) | Proposed solver (s) |
|---|---|---|
| Four-legged Stool | 5998 | 4744 |
| Fin | 11988 | 10342 |
| Lego cube | 18476 | 16780 |
| Maze design | 27540 | 25380 |
| ASTM tensile specimen | 680 | 608 |

### 5.2. Total printing time

Five 3D models chosen are manufactured using an in-house developed FDM 3D printer (RepRap with Marlin), employing G-codes generated by Cura software and the ACO method for build time evaluation, as illustrated in Fig. 10a–e. The entire process is monitored, and the time taken is recorded. The time taken to heat the printing bed and the nozzle is not accounted for time assessment. When the extruder moves away from its origin (0,0,0), the timer starts and ends when the nozzle exits the final printing.

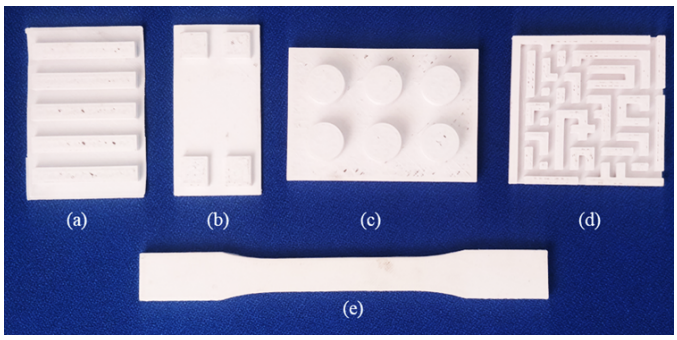


**Fig. 10.** 3D-printed case study models for build time comparison

Table 4, shows the actual printing time obtained for the implementation of G-codes of the Cura slicer and the ACO solver. From the observation, parts fabricated with the G-code generated by utilizing the ACO method result in a shorter printing time compared to the G-code developed via the Cura software. Table 4 shows that the ACO-generated G-code works effectively for the Four-legged stool model, resulting in a 21% reduction in build time compared to cura. The actual printing time

**Table 4**
Actual printing time (s)

| Model | Slicer software (s) | Proposed solver (s) |
|---|---|---|
| Four-legged stool | 5733 | 4479 |
| Fin | 12150 | 10800 |
| Lego cube | 18600 | 17136 |
| Maze design | 21006 | 19440 |
| ASTM tensile specimen | 867 | 816 |

of the fin model is 11% faster, as compared to Cura, followed by the Lego cube at 8%, the maze at 7%, and the ASTM specimen at 6%. When compared to the estimated printing (build) time, the actual build time of the parts differs by a small percentage [31]. This is because the estimated build time is calculated based on the preset acceleration and jerk settings on the slicer software, which differ from the FDM machine acceleration and jerk. Figure 11 shows the estimated and actual printing time obtained for G-code of the cura slicer and the ACO-generated G-code. It is evident from the graph that printing time of a part is also affected by the nozzle travel. The green line in the graph shows the experimental build time of the proposed ACO algorithm which significantly reduces the travel moves when compared to the Cura slicer. It is evident that by optimizing the travel motion of the nozzle the printing time of the models can be reduced.

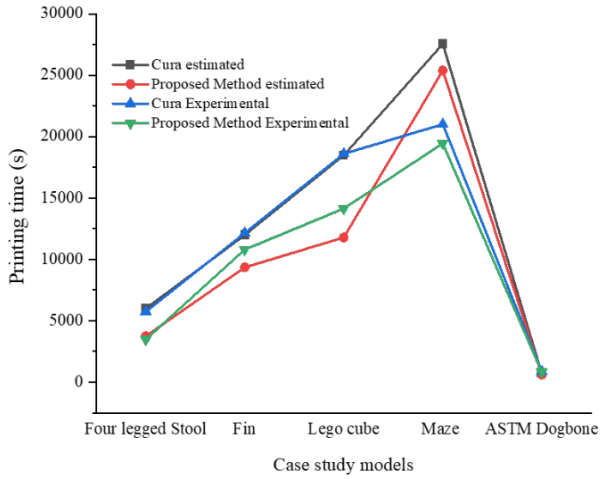


**Fig. 11.** Case study models printing time estimated and experimental

### 5.3. Strength

Table 5 shows the contribution of travel moves before and after the implementation of the ACO algorithm on strength the algorithm reduces the travel motion of the nozzle by more than 50%. The quality of the 3D-printed part is verified based on its strength and visual appearance. Figure 12a depicts the 3D-printed tensile specimen using the G-codes of the Cura slicer (T1, T2, and T3). Figure 12b shows the test specimens using ACO generated G-codes (T1, T2, and T3) subjected to a tensile test. It was found that the Cura slicer generated G-code results in a tensile strength of 15.5 MPa with a standard deviation ($\sigma$) of 0.75, whereas the G-code developed from the ACO algorithm results in a tensile strength of 16.3 MPa [32] with a standard deviation ($\sigma$) of 1.02, which is 5% more. Reducing travel can enhance the strength of a 3D-printed part in several ways: i. Reduced wrapping: by reducing travel, the printer will spend less time extruding material, which can help to reduce the chance of warping and enhance strength [33]. ii. Stronger bonds: When the nozzle head moves from one location to another at different speeds, faster deposition can create gaps in the printed part where the extruded material did not fully bond to the previous layer. By reducing travel, these gaps

can be minimized, which results in stronger bonds between layers of the printed part [34]. iii. Improved accuracy: reducing travel can also help to improve the dimensional accuracy of the printed part, as it reduces the chances of the printer head or bed shifting during the printing process can cause stringing effects [20]. According to the tensile test results, the strength of the 3D models was significantly improved by using the proposed method.

**Table 5**
Travel contribution on build time before and after optimization

| Model | Travel % | | |
|---|---|---|---|
| | Before ACO implementation | After ACO implementation | % Reduction in travel |
| Four-legged stool | 15 | 10 | 33 |
| Fin | 8 | 2 | 75 |
| Lego cube | 7 | 2 | 71 |
| Maze design | 19 | 8 | 57 |
| ASTM tensile specimen | 5 | 2 | 60 |

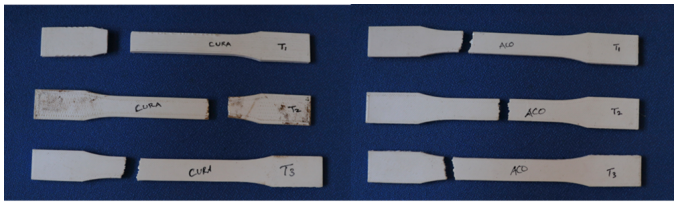


(a) (b)

**Fig. 12.** Validation of strength printed using G-codes generated by (a) Cura (b) proposed algorithm after the tensile test

### 5.4. Comparison of results with previous work

This section compares the previous works related to optimizing the travel movements of the nozzle and the comparison is shown in Table 6. To compare the results of the proposed algorithm with the results of the previous work, the proposed ACO method is applied to the 3D model "XYZ 20 mm calibration cube" from [35]. The model is sliced using the same printing parameters mentioned in [35] and the actual build time is used as the evaluation metric. The results showed that for the 3D model "XYZ 20 mm calibration cube" the build time is reduced by 4.2% by implementing the proposed ACO method when compared to [35]. Further the proposed method build time is compared with cura and it shows that the overall printing time of the 3D model is reduced by 30% which is a significant improvement in reduction of build time by optimizing the travel movement alone by using the proposed method. Thus the proposed ACO method performs well in terms of reducing the travel segments thereby the overall print time of a 3D model can be reduced. As compared to Cura, the mean estimated printing time was reduced by 12.2% on average compared to the proposed algorithm. According to the travel contribution given in Table 5, it can be observed that the travel segments were reduced by 60% on average using the proposed ACO method. The actual build time of the proposed method and cura were compared, it is observed that by using the proposed method the build time for model the "four legged stool" is reduced by 21%, followed by fin: 7%, lego cube: 8%, Maze: 7%, and ASTM specimen: 6%. From the tensile tests it is evident that the strength of the part fabricated using proposed method generated G-code has been increased by 5%, when compared to cura. To validate the performance of the proposed model according to Table 6, two references have been considered for the comparison of reduction in build time. It is evident that the proposed method performs well in terms reducing the travel segment of the nozzle which in turn reduces the build time of the printed part significantly.

**Table 6**
Comparison of similar studies

| Ref | Model used | Goal | Cura time (s) | Previous work build time [35] (s) | Proposed method build time (s) | % reduction |
|---|---|---|---|---|---|---|
| Un directed rural postman problem [35] | XYZ 20 mm calibration cube | Printing order | 2610 | 1899 | 1819.7 | 4.2 |

## 6. CONCLUSION

In a conventional 3D printer, printing (build) time is higher than the extruder travel (idle move) between segments as no material will be deposited on the layers. The paper presents a bioinspired optimization strategy based on ant colony optimization for reducing the part-build time on FDM-based machines. The optimization is based on a solution to the travelling salesman problem produced with ACO and an existing mathematical model to minimize the travel transitions of the nozzle is formulated. The optimal path developed by the ACO algorithm in terms of G-codes is compared with the G-codes developed from commercial slicer software. Comparison of the ACO G-code shows improvement, i.e., reduction of the travel of the nozzle by more than 50% on average. The average reduction of estimated build time is 12% and the actual build time is reduced by 11% and with an increase in strength of the printed part by 5% by the implementation of the ACO algorithm. Moreover, the advantage of ACO is that it is simple to implement and can find the shortest distance between nodes. The proposed work has been conducted within the scope of broader research in the development of systems that fabricates parts in less time. The work is aimed to address the main industrial demands such as faster part fabrication, i.e., mass production can be achieved using 3D printing.

## REFERENCES

[1] Ultimaker cura: Powerful, easy-to-use 3d printing software. [Online]. Available: https://ultimaker.com/software/ultimaker-cura

[2] A. Colorni, M. Dorigo, V. Maniezzo *et al.*, "Distributed optimization by ant colonies," in *Proceedings of the first European conference on artificial life*, vol. 142. Paris, France, 1991, pp. 134–142.

[3] Y. Weidong, "Optimal path planning in rapid prototyping based on genetic algorithm," in *2009 Chinese Control and Decision Conference*, 2009, pp. 5068–5072.

[4] Y. Li and S. Gong, "Dynamic ant colony optimisation for tsp," *Int. J. Adv. Manuf. Technol.*, vol. 22, pp. 528–533, 2003.

[5] J. Balic and M. Korosec, "Intelligent tool path generation for milling of free surfaces using neural networks," *Int. J. Mach. Tools Manuf.*, vol. 42, no. 10, pp. 1171–1179, 2002.

[6] P. Lechowicz, L. Koszalka, I. Pozniak-Koszalka, and A. Kasprzak, "Path optimization in 3d printer: algorithms and experimentation system," in *2016 4th International Symposium on Computational and Business Intelligence (ISCBI)*. IEEE, 2016, pp. 137–142.

[7] N. Volpato, R. Nakashima, L. Galvao, A. Barboza, P. Benevides, and L. Nunes, "Reducing repositioning distances in fused deposition-based processes using optimization algorithms," in *High Value Manufacturing: Advanced Research in Virtual and Rapid Prototyping: Proceedings of the 6th International Conference on Advanced Research in Virtual and Rapid Prototyping, Leiria, Portugal*, 2013, p. 417.

[8] B. Thompson and H.-S. Yoon, "Velocity-regulated path planning algorithm for aerosol printing systems," *J. Manuf. Sci. Eng.*, vol. 137, no. 3, 2015.

[9] J. Yuan, J. Du, Z. Ma, A. Liu, and Y. He, "An optimization approach for path planning of high-quality and uniform additive manufacturing," *Int. J. Adv. Manuf. Technol.*, vol. 92, no. 1-4, pp. 651–662, 2017.

[10] Y. Zhang, H. Li, T. Wang, B. Liu, and G. Wang, "A hybrid tool-path with no pause generation algorithm for 3d printing," in *J. Phys.-Conf. Ser.*, vol. 1754, no. 1. IOP Publishing, 2021, p. 012222.

[11] P.K. Wah, K.G. Murty, A. Joneja, and L.C. Chiu, "Tool path optimization in layered manufacturing," *IIE Trans.*, vol. 34, no. 4, pp. 335–347, 2002.

[12] A. Papacharalampopoulos, H. Bikas, and P. Stavropoulos, "Path planning for the infill of 3d printed parts utilizing hilbert curves," *Procedia Manuf.*, vol. 21, pp. 757–764, 2018.

[13] T. Liu, S. Yuan, Y. Wang, Y. Xiong, J. Zhu, L. Lu, and Y. Tang, "Stress-driven infill mapping for 3d-printed continuous fiber composite with tunable infill density and morphology," *Addit. Manuf.*, vol. 62, p. 103374, 2023.

[14] M. Dorigo and G. Di Caro, "Ant colony optimization: a new meta-heuristic," in *Proc. of the 1999 congress on evolutionary computation-CEC99 (Cat. No. 99TH8406)*, vol. 2. IEEE, 1999, pp. 1470–1477.

[15] B. Fox, W. Xiang, and H.P. Lee, "Industrial applications of the ant colony optimization algorithm," *Int. J. Adv. Manuf. Technol.*, vol. 31, pp. 805–814, 2007.

[16] W. Liu, L. Chen, G. Mai, and L. Song, "Toolpath planning for additive manufacturing using sliced model decomposition and metaheuristic algorithms," *Adv. Eng. Softw.*, vol. 149, p. 102906, 2020.

[17] K.-Y. Fok, C.-T. Cheng, N. Ganganath, H. H.-C. Iu, and K. T. Chi, "Accelerating 3d printing process using an extended ant colony optimization algorithm," in *2018 IEEE International Symposium on Circuits and Systems (ISCAS)*. IEEE, 2018, pp. 1–5.

[18] K.-Y. Fok, C.-T. Cheng, K. T. Chi, and N. Ganganath, "A relaxation scheme for tsp-based 3d printing path optimizer," in *2016 International Conference on Cyber-Enabled Distributed Computing and Knowledge Discovery (CyberC)*. IEEE, 2016, pp. 382–385.

[19] H. Liu, R. Liu, Z. Liu, and S. Xu, "Minimizing the number of transitions of 3d printing nozzles using a traveling-salesman-problem optimization model," *Int. J. Precis. Eng. Manuf.*, vol. 22, pp. 1617–1637, 2021.

[20] K.-Y. Fok, C.-T. Cheng, N. Ganganath, H.H.-C. Iu, and K.T. Chi, "An aco-based tool-path optimizer for 3-d printing applications," *IEEE Trans. Ind. Inform.*, vol. 15, no. 4, pp. 2277–2287, 2018.

[21] F. Hamzeh, F. El Sakka, M.H. Senan, and A.A. Yassin, "Optimizing 3d printing path to minimize the formation of weak bonds," in *Creative Construction Conference 2018*. Budapest University of Technology and Economics, 2018, pp. 181–188.

[22] H. Yin, S. Wang, Y. Wang, F. Li, L. Tian, X. Xue, and Q. Jia, "An intelligent 3d printing path planning algorithm 3d printing path planning algorithm: An intelligent sub-path planning algorithm," in *2021 the 5th International Conference on Innovation in Artificial Intelligence*, 2021, pp. 241–246.

[23] Matlab & simulink. [Online]. Available: https://in.mathworks.com/products/matlab.html

[24] Solidworks. [Online]. Available: https://www.solidworks.com

[25] 3d cad, cam, cae & pcb cloud-based software. [Online]. Available: https://www.autodesk.in/products/fusion-360

[26] Thingiverse – digital designs for physical objects. [Online]. Available: https://www.thingiverse.com

[27] R. Skinderowicz, "The gpu-based parallel ant colony system," *J. Parallel Distrib. Comput.*, vol. 98, pp. 48–60, 2016.

[28] K. J. Christiyan, U. Chandrasekhar, and K. Venkateswarlu, "A study on the influence of process parameters on the mechanical properties of 3d printed abs composite," in *IOP conference series: materials science and engineering*, vol. 114, no. 1. IOP Publishing, 2016, p. 012109.

[29] Standard test method for tensile properties of plastics, astm stand., vol. 08, pp. 1–15, 2014. [Online]. Available: https://www.astm.org/d0638-14.html

[30] Analyse your 3d printing g-code to provide accurate information such as print time and average speed. [Online]. Available: https://www.gcodeanalyser.com

[31] M. Kocisko, M. Teliskova, J. Torok, and J. Petrus, "Postprocess options for home 3d printers," *Procedia Eng.*, vol. 196, pp. 1065–1071, 2017.

[32] C. Dudescu and L. Racz, "Effects of raster orientation, infill rate and infill pattern on the mechanical properties of 3d printed materials," *Acta Univ. Cibiniensis-Tech. Ser.*, vol. 69, no. 1, pp. 23–30, 2017.

[33] M. S. Alsoufi and A. Elsayed, "Warping deformation of desktop 3d printed parts manufactured by open source fused deposition modeling (fdm) system," *Int. J. Mech. Mechatron. Eng*, vol. 17, no. 11, pp. 7–16, 2017.

[34] A. Abbott, G. Tandon, R. Bradford, H. Koerner, and J. Baur, "Process-structure-property effects on abs bond strength in fused filament fabrication," *Addit. Manuf.*, vol. 19, pp. 29–38, 2018.

[35] K.-Y. Fok, N. Ganganath, C.-T. Cheng, H. H.-C. Iu, and K. T. Chi, "A nozzle path planner for 3-d printing applications," *IEEE Trans. Ind. Inf.*, vol. 16, no. 10, pp. 6313–6323, 2019.